PAPER

Check for updates

Membrane destruction-mediated antibacterial activity of tungsten disulfide (WS₂)

Xu Liu,[ab] Guangxin Duan,[a] Weifeng Li, [ID] *[a] Zhufa Zhou*[b] and Ruhong Zhou [ID] *[acd]

The antibacterial activities of tungsten disulfide (WS₂) nanosheets against two representative bacterial strains: Gram-negative *Escherichia coli* (*E. coli*) and Gram-positive *Staphylococcus aureus* (*S. aureus*) were evaluated by colony-forming unit (CFU) studies. The WS₂ samples demonstrate a time and concentration dependent antibacterial activity (retardation of bacterial growth) for both bacterial strains. Morphology analyses reveal that WS₂ nanosheets adhere to the bacterial surfaces, resulting in robust inhibition of cell proliferation once a bacterium is fully covered with this nanomaterial. More importantly, the intimate contact of WS₂ nanosheets with a bacterium cell membrane can cause serious damage to the membrane integrity, and subsequently the cell death. On the other hand, the reactive oxygen species (ROS) generated by WS₂ nanosheets are found to be modest regardless of the WS₂ concentration, which is contradictory to the case of its structural analogue, MoS₂, where ROS also play a significant role in its antibacterial activity. Taken together, our findings provide a detailed understanding of the antibacterial mechanism of WS₂ nanosheets, which might help promote their potential applications in biomedical fields.

1. Introduction

Two dimensional (2D) nanomaterials, such as graphene and its derivatives, have attracted considerable attention in recent years with wide applications in electronic and optical devices,[1,2] drug and gene delivery vehicles,[3–7] as well as cancer therapeutic platforms.[8–12] After graphene, the first family member of these 2D nanomaterials, a number of other such nanomaterials have been discovered including phosphorene, silicene and transition metal dichalcogenides (TMDCs).[13] Among them, the TMDCs, such as WS₂, MoS₂, WSe₂, exhibit a considerably high structural stability, with a melting point reaching up to 1185 °C. They have been explored for applications in field-effect transistors,[14] lithium-ion batteries,[15,16] integrated circuits,[17] gas sensors,[18] hydrogen evolution[19] and phototransistors.[20]

In particular, the potential antibacterial capabilities of these 2D-nanomaterials have raised considerable interest in recent years.[21–23] For instance, graphene (and graphene oxide) has been systematically studied[24] for its antimicrobial activities,[25–28] along with its underlying molecular mechanisms.[29–32] It was revealed that graphene and graphene oxide nanosheets can cut into cell membranes,[32] extract large amount of phospholipids,[32] and create holes (pores) on cell membranes,[33] through large scale molecular dynamics simulations.[34–38]

Compared to graphene and its derivatives, however, there has been much less studies on the antibacterial activities of TMDCs. In 2014, Yang *et al.*[39] examined the antibacterial capability of MoS₂ and found that MoS₂ nanosheets are much more potent than its raw powders. The reasons proposed for this were: (i) MoS₂ nanosheets are capable of inducing stronger superoxide anion-independent oxidative stress than raw powders; and (ii) MoS₂ nanosheets provide more effective contact areas with the bacteria, which both helped to cause more dramatic membrane stresses in the nanosheet form. Meanwhile, Choi group demonstrated the antibacterial activities of WSe₂ nanosheets (in the form of WSe₂-ssDNA by exfoliation) mainly through the induction of ROS-independent oxidative stress.[22] Shinde and co-workers also demonstrated that WS₂ can cause retardation in bacterial growth and inhibitory effect on bacterial strains.[40] On the other hand, there are also conflicting reports in literature regarding these TMDCs' antibacterial activities. For instance, Chae and coworkers suggested that MoS₂ and WS₂ only displayed limited cytotoxicity and genotoxicity, with no significant deleterious effect to cellular viability.[41]

To help resolve some of these apparent discrepancies and also explore deeper the underlying mechanisms, we investigated the antibacterial activity of tungsten disulfide (WS₂) against two representative bacterial strains: Gram-negative *Escherichia coli* (*E. coli*) and Gram-positive *Staphylococcus aureus* (*S. aureus*) using the colony-forming units (CFU) method.

[a]*Institute of Quantitative Biology and Medicine, SRMP and RAD-X, Collaborative Innovation Center of Radiation Medicine of Jiangsu Higher Education Institutions, Soochow University, Suzhou 215123, China. E-mail: wfli@suda.edu.cn; ruhongz@us.ibm.com*

[b]*College of Chemistry, Chemical Engineering and Material Science, Soochow University, Suzhou 215123, China. E-mail: zhouzhufa@suda.edu.cn*

[c]*Computational Biological Center, IBM Thomas J. Watson Research Center, Yorktown Heights, NY 10598, USA*

[d]*Department of Chemistry, Columbia University, New York, NY 10027, USA*

We further examined the ROS generation with an oxidant-sensitive DCFH-DA probe and monitored the morphological changes of the bacteria with scanning electron microscope (SEM) and transmission electron microscopy (TEM). We found that the WS$_2$ nanosheets demonstrate a clear cytotoxicity to both *E. Coli* and *S. aureus* bacterial strains. Notably, only limited toxicity was observed in the eukaryotic cells with the control experiments. As revealed from the SEM and TEM results, the WS$_2$ nanosheets can form intimate contacts with the bacteria membranes by adhering onto them. Severe structural damages were observed on these cell membranes, eventually leading to bacterial cell deaths. WS$_2$ is found to be incapable of catalyzing the ROS generation which is in contrast to MoS$_2$. Thus, the antibacterial activity of WS$_2$ nanosheets is mainly attributed to the direct contact of WS$_2$ to the bacteria membrane which causes severe membrane disruption and thus the loss of structural integrity.

2. Methods and materials

2.1 Material preparation and characterization

The WS$_2$ powders were purchased from Nanjing XFNANO Materials Tech Company limited. The WS$_2$ nanosheets were prepared by the surfactant exfoliation method as reported in previous literature.[42] The morphology of single-layer WS$_2$ nanosheets was studied by using Veeco AFM in the tapping mode at the scanning rate of 1 Hz under ambient conditions. The topologies of the samples were further examined by transmission electron microscopy (TEM, Tecnai G220).

2.2 Bacterial cell preparation and antibacterial activity

Gram-negative bacteria *E. coli* (ATCC25922) and Gram-positive bacteria *S. aureus* (ATCC25923) were obtained from the American Type Culture Collection (ATCC, Rockville, Maryland, USA) and used as the model organisms for antibacterial experiments. Bacteria cells were first grown overnight in LB medium (Luria–Bertani) at 37 °C and harvested at the mid-exponential growth phase *via* centrifugation. Then they were washed three times to remove the residual growth-medium constituents and re-suspended in the sterile saline solution (0.9% NaCl). A portion of the bacterial suspension was diluted to around 1 × 10^6 CFU mL^{-1} for antibacterial evaluation. The cells used in all experiments are in the mid-exponential growth phase.

The WS$_2$ nanosheets samples were diluted to a concentration of 0, 25, 50, 100 and 200 μg mL^{-1}, respectively, using culture medium with a final concentration of bacteria of 1 × 10^6 CFU mL^{-1}. Both *E. coli* and *S. aureus* were cultured at the condition of 37 °C for up to 6 h. Antibacterial ability was evaluated by the colony counting method. In brief, the incubation bacterial solutions were initially diluted to 1 × 10^4 CFU mL^{-1}. Later, 100 μL of the diluted bacterial cells was spread on the solid LB agar plates. After incubation overnight at 37 °C, colonies on the plates were counted and compared with those on the control plates (without any WS$_2$ nanosheets) to calculate the loss of viability caused by the WS$_2$ nanosheets samples. The reported data were the average value of three separate similar runs.

2.3 Visualization of bacterial morphology

Morphological changes of the bacterial morphology were investigated by scanning electron microscopy (SEM) and transmission electron microscopy (TEM). The *E. coli* and *S. aureus* were incubated with WS$_2$ nanosheets for 2 h at the concentration of 100 μg mL^{-1}, respectively. Subsequently, 10 mL of bacterial suspensions were harvested by centrifugation at 6000 rpm. After quickly fixed with 2.5% glutaraldehyde and post fixed with 1% osmium tetroxide, the bacterial cells were dehydrated by using an ascending ethanol series (30%, 50%, 70%, 80%, 90%, 95% and 100%). The samples were then dehydrated overnight, followed by sputter-coated with platinum and mounted for SEM.

2.4 Reactive oxygen species (ROS) generation measurement

In order to analyze the generation of ROS induced by WS$_2$ nanosheets, an oxidant-sensitive dye 2′,7′-dichlorofluorescein diacetate (DCFH-DA, Invitrogen detection technologies, USA) was used following the method previously described.[43,44] Briefly, 25 μL 0.1 mM DCFH-DA was treated with 100 μL 0.01 N NaOH for 1 h to generate DCFH, followed by adding 375 μL 0.1 M PBS to terminate this reaction. Next, the WS$_2$ nanosheet samples were added to make the final concentrations: 0, 25, 50, 100 and 200 μg mL^{-1}. After 1 h reaction, the ROS generation was analyzed by a microplate reader at 485 nm excitation and 530 nm emission.

2.5 *In vitro* cytotoxicity to eukaryotic cells

In order to further evaluate the WS$_2$ cytotoxicity for eukaryotic cells, adenocarcinomic human alveolar basal epithelial cell line (A549) and human liver cancer cell line (HEP G2) were obtained from the American Type Culture Collection (ATCC, Rockville, Maryland, USA) and respectively cultured with WS$_2$ nanosheets by using the Cell Counting Kit-8 (CCK-8).[45] Briefly, A549 cells and HEP G2 cells were seeded in a 96-well cell culture plates at the densities of 5 × 10^3 cell per well, respectively, in DMEM containing 10% FBS at 37 °C in a humid atmosphere of 95% air and 5% CO$_2$ for 24 h. After 24 h incubation, cells reached ~80% confluence. Subsequently, the cells were incubated with WS$_2$ in serum-free medium, following a similar protocol used in our previous studies,[37] with WS$_2$ concentrations 12.5, 25, 50, 100, and 200 μg mL^{-1}. The cells cultured in the medium without any nanomaterials were used as the control. After another 24 h of incubation, the cells were washed with a D-Hanks buffer solution for two times, followed by adding the CCK-8 reagent (10 μL). After incubated for additional 2 h at 37 °C, the spectro photometrical absorbance of each well was measured at 450 nm wavelength on a microplate reader to calculate the changes of cell viability caused by the WS$_2$ nanosheets. Three replicates were done for each treatment group.

2.6 Statistical analysis

All the cell viability tests (Fig. 2c and d and 6) and ROS level results (Fig. 3) were obtained from experiments in triplicates.

The results are presented as average with standard deviation as error bars.

3. Results and discussion

3.1 Material characterization

The morphology of the WS_2 nanosheets was examined with atomic force microscopy (AFM) and transmission electron microscopy (TEM) first. Fig. 1a depicts the AFM image of the exfoliated WS_2 deposited on a mica substrate. The WS_2 nanosheets display a flat nanosheet structure coating on the mica surface. The thickness of the WS_2 nanosheets is accessed through constructing the height profile diagram along the transverse direction on the mica surface (labeled in Fig. 1a) and the result is shown in Fig. 1b. The exfoliated WS_2 samples are observed to have a typical thickness of ~1 nm, corresponding to around 2–3 layers of WS_2 sheets, indicating that the WS_2 sheets were well prepared. The TEM images are further taken for the WS_2 nanosheets deposited on the glass substrate to give a clearer view of their morphologies (Fig. 1c). The WS_2 nanosheets are seen densely packed on the glass surface adopting random orientations.

3.2 Antibacterial test

The bactericidal activities of WS_2 were evaluated against *E. coli* (Gram-negative) and *S. aureus* (Gram-positive) as two representative bacteria strains. *E. coli* and *S. aureus* were incubated with the dispersant of the WS_2 nanosheets at concentrations ranging from 25–250 μg mL^{-1} at 37 °C under 250 rpm shaking speed for 2 h and 6 h. Bacteria incubated at same conditions but without the WS_2 nanosheets treatment was used as a control. The death rate of the bacterial cells was determined by the colony counting method.

Fig. 2 summarizes the bacteria viability treated with the WS_2 sheets which demonstrate clear bacteria death for both *E. coli* and *S. aureus*. The viability of bacteria cells dramatically decreased with the increase of the WS_2 concentration and the incubation time. In detail, after treated with 25, 50, 100 and 200 μg mL^{-1} WS_2 for 2 h, the viability of *E. coli* was estimated to be 52.3%, 12.3%, 0% and 0%, respectively. The *E. coli* survival rate was further reduced at longer incubation time of 6 h. The same trend was also observed for the *S. aureus*. The viability of *S. aureus* was 84.1%, 18.0%, 4.3% and 0% after treated with WS_2 at concentrations of 25, 50, 100 and 200 μg mL^{-1} for 2 h. These results suggest that the WS_2 nanosheets could effectively kill bacteria in a concentration and time dependent manner.

3.3 Reactive oxygen species (ROS) generation analysis

As a structural analogue to WS_2, another TMDC family member, MoS_2, also demonstrates clear antibacterial activity.[39] The antibacterial activity for MoS_2 is found to be induced mainly by two factors: (1) MoS_2-bacteria direct contact induced membrane destruction and (2) oxidative stress caused by ROS (generated by MoS_2 nanosheets). To probe the possibility of ROS generation by WS_2 for its toxicity, we further examined the ROS level to examine whether the bacterial death was caused by oxidative damage using the DCFH-DA probe. DCFH-DA probe without WS_2 nanosheets was used as a negative control to validate our tests. The results are shown in Fig. 3. For WS_2 concentrations from 25 to 100 μg mL^{-1}, the fluorescence intensity only slightly increased, which is distinct to the dramatic decrease of the bacteria viability after 25 μg mL^{-1} in Fig. 2. The absence of strong ROS indicates that the oxygen stress was not the main reason for antibacterial activity of WS_2 nanosheets.

3.4 SEM and TEM analyses of bacteria morphology

After excluding the ROS generation of WS_2 for its antibacterial activity, it is anticipated that the direct contact of WS_2 with bacteria membrane and their subsequent interactions might play a key role. Our previous study[32] on graphene did show that the destruction of the membrane of bacteria (caused by direct contact of graphene and membrane) is a major reason for the bacteria death. To examine whether this is also the case for WS_2, the morphological changes of both bacterial cells, *E. coli* and *S. aureus*, were accessed using SEM images.
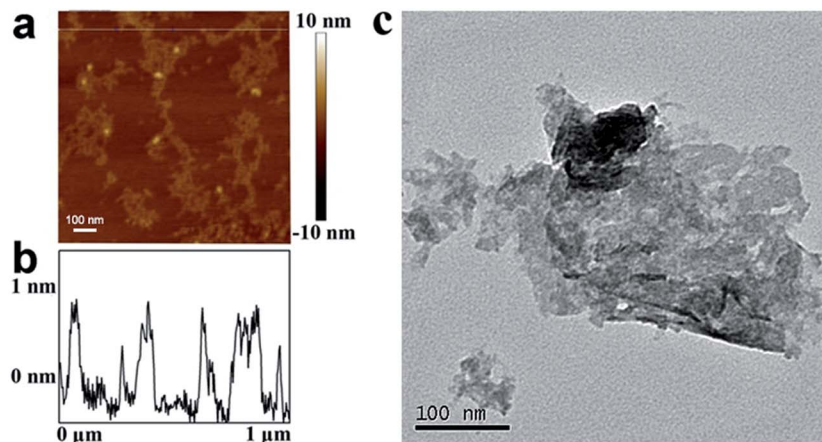

Fig. 1 (a) Atomic force microscopy images of the WS_2 nanosheets deposited on silica substrate, (b) the height profile diagram along the line labelled in (a). (c) Transmission electron microscopy image of one WS_2 nanosheet.
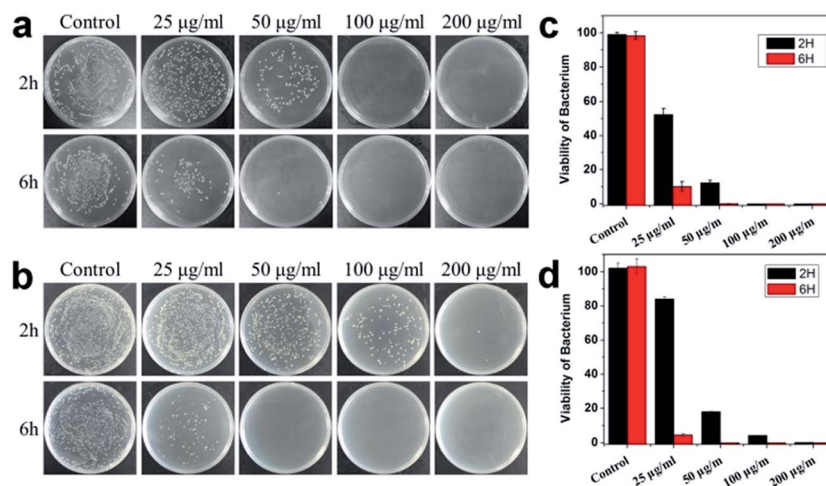
Fig. 2 Antibacterial activity of WS$_2$ nanosheets. (a and c) Viability of *E. coli* after treated with WS$_2$ nanosheets for 2 and 6 h. (b and d) Viability of *S. aureus* after treated with WS$_2$ nanosheets for 2 and 6 h.
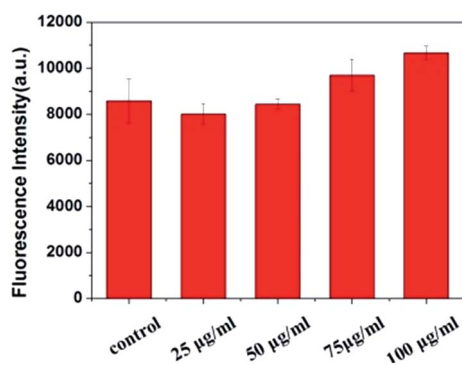

Fig. 3 Concentration-dependent ROS generation induced by WS$_2$ nanosheets was analyzed by DCFH-DA probe. Three replicate samples have been tested for error analyses.

Under the control experiment without the WS$_2$ nanosheets treatment, *E. coli* exhibited normal rod-like morphology with smooth and intact membranes (Fig. 4a). However, once incubated with WS$_2$ nanosheets for 2 h, severe deformations were observed for *E. coli* cells with their structural damages indicated by arrows in Fig. 4b. Notably, the cell shape became longer and some of them were even drilled, accompanied by formation of large cavities on the surfaces, which is consistent with what we have observed for graphene.[33] Fig. 4c displays another example with the *E. coli* cell shape even more seriously distorted and its cell membrane greatly ruptured.

Similar phenomena were observed for *S. aureus*. The overall morphology of *S. aureus* cells changed from regular sphere shape (the control data, Fig. 4d) to irregular shape (Fig. 4e and f) after incubated with WS$_2$ nanosheets for 2 h, with serious damages on the cell walls indicated by arrows.

Comparing the WS$_2$ treated *E. coli* and *S. aureus* SEM images (Fig. 4b, c, e and f) with control data (Fig. 4a and d), the most significant changes are that the surfaces of dead bacteria are very rich in plate-like particles with sharp edges, indicating that these cell surfaces are mostly likely covered by massive WS$_2$ nanosheets. In addition to the disruption of the cell membranes, these covering WS$_2$ nanosheets might also block various membrane channels and thus cause malfunction of
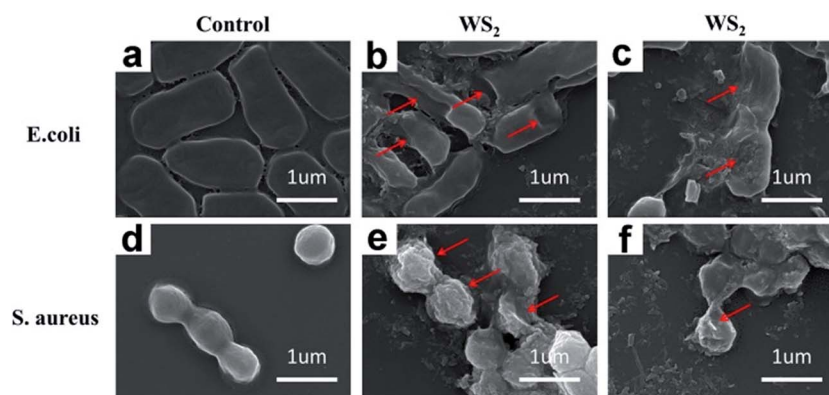

Fig. 4 SEM images of (a) *E. coli* control (without nanosheets); (b) and (c) *E. coli* treated with 100 μg mL^{-1} of WS$_2$; (d) *S. aureus* control (without nanosheets); (e) and (f) *S. aureus* treated with 100 μg mL^{-1} of WS$_2$. The distorted morphology of the bacteria is indicated by the red arrows.

selective permeable barriers. This was also suggested for graphene oxide (GO) by Akhavan *et al.*, where GO nanosheets were speculated to prevent the bacteria from exchanging materials with the environment by blocking various membrane channels.[46]

Overall, these SEM images clearly indicate that the irreversible damages are induced on bacterial cells because of their direct contact with WS_2 nanosheets. Similar mechanisms were proposed previously by many other groups,[47–49] with graphene and/or carbon nanotubes, where serious destructions on cell membranes result in membrane stresses and subsequent bacterial cell deaths.

It should be noted that in a previous study, Chae and coworkers suggested that WS_2 only displayed limited cytotoxicity and genotoxicity, with no significant deleterious effect to cellular viability.[41] However, our present study demonstrates a clear antibacterial activity of WS_2 to both *E. coli* and *S. aureus*. This apparent discrepancy was first from the fact that Chae and coworkers used human epithelial kidney cells (HEK293f),[41] *i.e.* one type of eukaryotic cells, which we also found limited cytotoxicity (more below). Another contribution to this apparent discrepancy is from the morphology of the WS_2 samples. The WS_2 sheets prepared by Chae was considerably larger and thicker (around 8–10 μm in diameter and 5–8 layers in thickness) than that used in our current study. As characterized in Fig. 1, our WS_2 nanosheets have a diameter of ∼100 nm

uniformly, and are well separated to be monolayers. These mostly monolayer nanosheets (sharp and free-floating) are expected to interact with the cell membrane in a stronger manner, thus resulting in more membrane stress and destruction. We noticed that such a morphology-dependent cytotoxicity was also previously observed for MoS_2 and graphene. Pumera and coworkers reported that the deleterious cytotoxic effects of MoS_2 become stronger when the MoS_2 nanosheets are better exfoliated.[50] Another study by Liao *et al.* also indicated that graphene and graphene oxide are robust in slicing red blood cells when they are in monolayers.[51] This is believed to be caused by the increase in specific surface areas and sharp edges of MoS_2 and graphene nanosheets.

The direct contact of WS_2 with bacteria membrane is further confirmed by TEM images. As shown in Fig. 5a, two WS_2 particles are found to adhere to *E. coli* surface, one of which has already penetrated into the membrane to a certain extent. Fig. 5b depicts numerous *E. coli* bacteria where WS_2 particles are commonly found at the bacteria interfacial and corner regions. Overall, Fig. 5a and b represent an earlier stage of *E. coli* interaction with WS_2. During this stage, the bacteria still demonstrate a rod-like morphology with smooth surface although local deformations can be observed at the WS_2 binding site (as indicated in Fig. 5a).

After 2 h incubation, severe loss of structural integrity was observed for *E. coli* bacteria. Fig. 5c depicts one *E. coli* bacterium
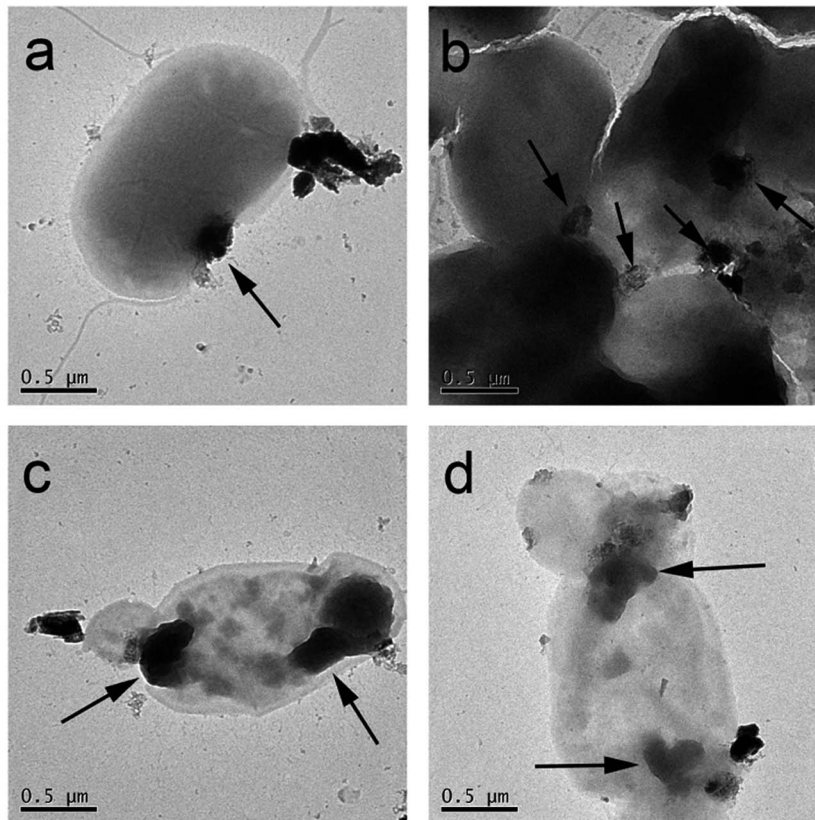

Fig. 5 TEM images of *E. coli* treated with 100 μg mL^{-1} of WS_2. (a) and (b) were taken immediately after the WS_2 treatment, while (c) and (d) were taken after 2 h incubation. The WS_2 particles are indicated by the black arrows.

interacting with WS_2 sheets at two ends of the cell. Clear structural deformations were observed which are mostly uniform at the WS_2 binding sites (indicated by arrows in Fig. 5c). Similar phenomenon is seen in Fig. 5d where WS_2 binds to two regions of cell membrane and causes severe membrane damage. The cell morphologies in Fig. 5c and d have been greatly changed compared to those in Fig. 5a and b, indicating that the cell membrane damages are irreversible and fatal. In addition, the cell proliferation is also found to be totally inhibited for these damaged cells (Fig. 5c and d) during the entire incubation process (other TEM images showed similar behavior on the proliferation process of other damaged cells). This inhibition of cell proliferation by nanomaterial coverage was also reported by Akhavan et al. on graphene toxicity towards E. coli.[46] Thus, one can conclude that the damage of cell morphology (and subsequent proliferation) is initiated by the direct contact with WS_2 nanosheets.

3.5 In vitro cytotoxicity to eukaryotic cells

To further test the potential cytotoxicity of WS_2 nanosheets to eukaryotic cells, we used the A549 and HEP G2 cells as two representatives. These two cells are commonly used to evaluate the cytotoxicity of several widely-studied nanomaterials in the recent years, such as graphene oxide,[52] MoS_2,[53] Ag nanoparticles[54] and single walled carbon nanotubes.[55] The viability of the A549 and HEP G2 cells were examined after exposure to the WS_2 nanosheets by the CCK-8 assay. First, A549 and HEP G2 cells were incubated in complete culture medium containing 10% FBS. After 24 h incubation, the cells reached ∼80% confluence. Then, these cells were treated with WS_2 nanosheets in serum-free medium. The cell viability losses were also observed for both A549 and HEP G2 cells despite that they were less significant than the bacteria. As shown in Fig. 6a and b, the cell viability kept almost a constant at low WS_2 concentration (12.5 and 25 $\mu g\ mL^{-1}$), although a slight decrease was detected for HEP G2. Further increasing of the WS_2 concentration would induce severe loss of the cell viability. In addition, the loss of A549 cells viability is systematically higher than HEP G2, which is 30%, 43%, and 51% at the WS_2 concentrations of 50, 100 and

200 $\mu g\ mL^{-1}$ respectively (Fig. 6a). In comparison, the loss of HEP G2 cells viability was lower, which are 22%, 23% and 26% at the WS_2 concentrations of 50, 100 and 200 $\mu g\ mL^{-1}$, respectively (Fig. 6b). Generally, WS_2 displays a significantly lower cytotoxicity to eukaryotic cells as compared to both Gram-negative and Gram-positive bacteria. This result is consistent with antibacterial studies of other 2D nanomaterials like GO.[56] The lower cytotoxicity to eukaryotic cells than bacteria seems to be a common feature for the nanomaterials. While a well-documented mechanism is still absent, a possible reason is proposed to be the existence of nuclear membrane in eukaryotic cells. In addition, as suggested from our previous studies,[57] biomolecules like proteins can rapidly adsorb onto nanomaterial surfaces to form protein corona which can effectively reduce their cytotoxicity. In our current study, WS_2 nanosheets were probably partially coated with protein FBS in the cell viability assays, even though the culture media of A549 and HEP G2 cells were replaced with WS_2-loaded serum-free media after reaching ∼80% confluence.[57,58] In other words, our current A549 and HEP G2 cell experiments are more similar to Chae and coworkers' experiment on HEK293f as mentioned above. On the contrary, in the antibacterial experiments, the WS_2 nanosheets were kept "naked" during the entire incubation with bacteria.

It is worth noticing that WS_2 also exhibits considerably lower toxicity than graphene and graphene derivatives (even at the high WS_2 concentration of 200 $\mu g\ mL^{-1}$).[59] The reason for the more benign toxicity than graphene is caused by the distinct chemical structures of the two materials. For WS_2, there is intrinsic electron transfer from W to S atoms on the nanosheet, making WS_2 somewhat more hydrophilic. While for graphene (graphene oxide also has large un-oxidized sp^2 domains on its surface), it is more hydrophobic; and meanwhile, its unique compact structure possesses strong dispersion interactions with other molecules such as phospholipids. Thus, the interactions between graphene and lipids are so strong that it not only causes graphene penetration into cell membranes but also results in destructive extraction of lipids from cell membranes.[32]
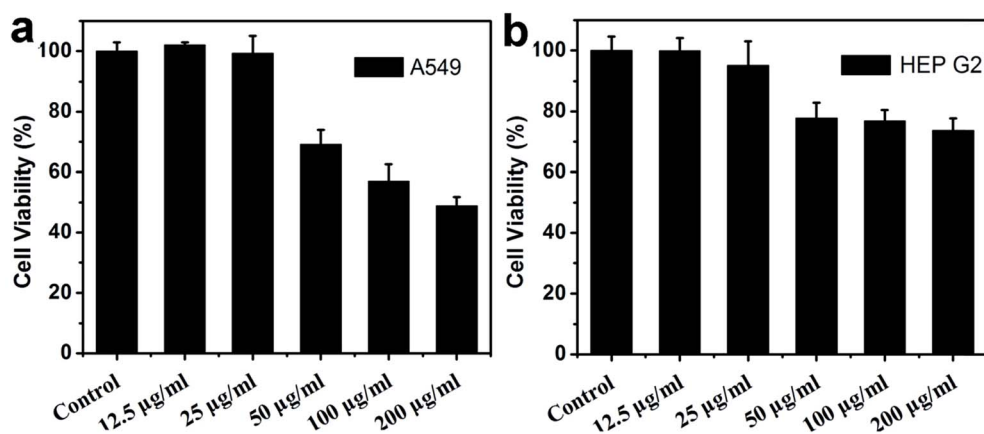

Fig. 6 Cell viability of A549 (a) and HEP G2 (b) as measured using CCK 8 method, following 24 h exposure to varying amounts of WS_2.

4. Conclusion

The antibacterial activity of the tungsten disulfide (WS₂) nano-sheets was evaluated by the colony counting method. It was found that WS₂ nanosheets exhibit a remarkable antibacterial activity towards both *E. coli* (Gram-negative) and *S. aureus* (Gram-positive). The viability of bacteria cells dramatically decreases with the increase of the WS₂ concentration and incubation time. As observed by the SEM and TEM images, the WS₂ nanosheets could easily cover cells to prevent bacteria from proliferating and induce structural damage. Meanwhile, our results reveal that the ROS generated by WS₂ is very modest. Thus, the antibacterial activity of WS₂ nanosheets is mainly attributed to the loss of structural integrity of bacterial membrane that is induced by direct contact with the nano-material instead of oxidative stress observed in the case of graphene. This study, thus, sheds light on the antibacterial activity of the WS₂ nanosheets and promotes further research of the TMDC materials for bio-medical applications.

Author contributions

R. H. Z., and X. L. conceived and designed the experiments. X. L., and G. D. performed the antibacterial experiments. X. L., G. D., W. F. L., and R. H. Z. analyzed the data. X. L., W. F. L, Z. Z. and R. H. Z. co-wrote the paper. All authors discussed the results and commented on the manuscript.

Conflict of interest

The authors declare no competing financial interests. Correspondence and requests for materials should be addressed to R. H. Z.

Acknowledgements

References

1 F. Xia, H. Wang, D. Xiao, M. Dubey and A. Ramasubramaniam, *Nat. Photonics*, 2014, **8**, 899–907.

2 G. Fiori, F. Bonaccorso, G. Iannaccone, T. Palacios, D. Neumaier, A. Seabaugh, S. K. Banerjee and L. Colombo, *Nat. Nanotechnol.*, 2014, **9**, 768–779.

3 S. Goenka, V. Sant and S. Sant, *J. Controlled Release*, 2014, **173**, 75–88.

4 M. Karimi, A. Ghasemi, P. Sahandi Zangabad, R. Rahighi, S. M. Moosavi Basri, H. Mirshekari, M. Amiri, Z. Shafaei Pishabad, A. Aslani, M. Bozorgomid, D. Ghosh, A. Beyzavi, A. Vaseghi, A. R. Aref, L. Haghani, S. Bahrami and M. R. Hamblin, *Chem. Soc. Rev.*, 2016, **45**, 1457–1501.

5 J. Liu, L. Cui and D. Losic, *Acta Biomater.*, 2013, **9**, 9243–9257.

6 K. Yang, L. Feng and Z. Liu, *Expert Opin. Drug Delivery*, 2015, **12**, 601–612.

7 T. Liu, C. Wang, X. Gu, H. Gong, L. Cheng, X. Shi, L. Feng, B. Sun and Z. Liu, *Adv. Mater.*, 2014, **26**, 3433–3440.

8 M. Orecchioni, R. Cabizza, A. Bianco and L. G. Delogu, *Theranostics*, 2015, **5**, 710–723.

9 M. Li, A. Zhao, K. Dong, W. Li, J. Ren and X. Qu, *Nano Res.*, 2015, **8**, 3216–3227.

10 Z. Huang, Y. Qi, D. Yu and J. Zhan, *RSC Adv.*, 2016, **6**, 31031–31036.

11 Z. Lei, W. Zhu, S. Xu, J. Ding, J. Wan and P. Wu, *ACS Appl. Mater. Interfaces*, 2016, **8**, 20900–20908.

12 Q. Liu, C. Sun, Q. He, A. Khalil, T. Xiang, D. Liu, Y. Zhou, J. Wang and L. Song, *Nano Res.*, 2015, **8**, 3982–3991.

13 H. Zhang, *ACS Nano*, 2015, **9**, 9451–9469.

14 C. Gong, H. Zhang, W. Wang, L. Colombo, R. M. Wallace and K. Cho, *Appl. Phys. Lett.*, 2013, **103**, 053513.

15 Z. Luo, J. Zhou, L. Wang, G. Fang, A. Pan and S. Liang, *J. Mater. Chem. A*, 2016, **4**, 15302–15308.

16 H. Yoo, A. P. Tiwari, J. Lee, D. Kim, J. H. Park and H. Lee, *Nanoscale*, 2015, **7**, 3404–3409.

17 R. Cheng, S. Jiang, Y. Chen, Y. Liu, N. Weiss, H.-C. Cheng, H. Wu, Y. Huang and X. Duan, *Nat. Commun.*, 2014, **5**, 5143.

18 D. Sarkar, X. Xie, J. Kang, H. Zhang, W. Liu, J. Navarrete, M. Moskovits and K. Banerjee, *Nano Lett.*, 2015, **15**, 2852–2862.

19 A. Ambrosi, Z. Sofer and M. Pumera, *Chem. Commun.*, 2015, **51**, 8450–8453.

20 W. Zhang, M.-H. Chiu, C.-H. Chen, W. Chen, L.-J. Li and A. T. S. Wee, *ACS Nano*, 2014, **8**, 8653–8661.

21 T. I. Kim, B. Kwon, J. Yoon, I.-J. Park, G. S. Bang, Y. Park, Y.-S. Seo and S.-Y. Choi, *ACS Appl. Mater. Interfaces*, 2017, **9**, 7908–7917.

22 G. S. Bang, S. Cho, N. Son, G. W. Shim, B.-K. Cho and S.-Y. Choi, *ACS Appl. Mater. Interfaces*, 2016, **8**, 1943–1950.

23 X. Li, J. Shan, W. Zhang, S. Su, L. Yuwen and L. Wang, *Small*, 2017, **13**, 1602660.

24 F. Perreault, A. F. de Faria, S. Nejati and M. Elimelech, *ACS Nano*, 2015, **9**, 7226–7236.

25 L. Shi, J. Chen, L. Teng, L. Wang, G. Zhu, S. Liu, Z. Luo, X. Shi, Y. Wang and L. Ren, *Small*, 2016, **12**, 4165–4184.

26 S. Szunerits and R. Boukherroub, *J. Mater. Chem. B*, 2016, **4**, 6892–6912.

27 Z. Liu, J. T. Robinson, X. Sun and H. Dai, *J. Am. Chem. Soc.*, 2008, **130**, 10876–10877.

28 L. Xiao, J. Sun, L. Liu, R. Hu, H. Lu, C. Cheng, Y. Huang, S. Wang and J. Geng, *ACS Appl. Mater. Interfaces*, 2017, **9**, 5382–5391.

29 J. D. Mangadlao, C. M. Santos, M. J. L. Felipe, A. C. C. de Leon, D. F. Rodrigues and R. C. Advincula, *Chem. Commun.*, 2015, **51**, 2886–2889.

30 S. Gurunathan, J. W. Han, A. A. Dayem, V. Eppakayala and J.-H. Kim, *Int. J. Nanomed.*, 2012, **7**, e14.

31 S. Liu, T. H. Zeng, M. Hofmann, E. Burcombe, J. Wei, R. Jiang, J. Kong and Y. Chen, *ACS Nano*, 2011, **5**, 6971–6980.

32 Y. Tu, M. Lv, P. Xiu, T. Huynh, M. Zhang, M. Castelli, Z. Liu, Q. Huang, C. Fan, H. Fang and R. Zhou, *Nat. Nanotechnol.*, 2013, **8**, 594–601.

33 G. Duan, Y. Zhang, B. Luan, J. K. Weber, R. W. Zhou, Z. Yang, L. Zhao, J. Xu, J. Luo and R. Zhou, *Sci. Rep.*, 2017, **7**, 42767.

34 R. Zhou, B. J. Berne and R. Germain, *Proc. Natl. Acad. Sci. U. S. A.*, 2001, **98**, 14931–14936.

35 P. Das, J. Li, A. K. Royyuru and R. Zhou, *J. Comput. Chem.*, 2009, **30**, 1654–1663.

36 Z. Xia, P. Clark, T. Huynh, P. Loher, Y. Zhao, H. W. Chen, I. Rigoutsos and R. Zhou, *Sci. Rep.*, 2012, **2**, 569.

37 Y. Chong, C. Ge, Z. Yang, J. A. Garate, Z. Gu, J. K. Weber, J. Liu and R. Zhou, *ACS Nano*, 2015, **9**, 5713–5724.

38 B. Luan, T. Huynh, L. Zhao and R. Zhou, *ACS Nano*, 2015, **9**, 663–669.

39 X. Yang, J. Li, T. Liang, C. Ma, Y. Zhang, H. Chen, N. Hanagata, H. Su and M. Xu, *Nanoscale*, 2014, **6**, 10126–10133.

40 G. R. Navale, C. S. Rout, K. N. Gohil, M. S. Dharne, D. J. Late and S. S. Shinde, *RSC Adv.*, 2015, **5**, 74726–74733.

41 J. H. Appel, D. O. Li, J. D. Podlevsky, A. Debnath, A. A. Green, Q. H. Wang and J. Chae, *ACS Biomater. Sci. Eng.*, 2016, **2**, 361–367.

42 R. J. Smith, P. J. King, M. Lotya, C. Wirtz, U. Khan, S. De, A. O'Neill, G. S. Duesberg, J. C. Grunlan, G. Moriarty, J. Chen, J. Wang, A. I. Minett, V. Nicolosi and J. N. Coleman, *Adv. Mater.*, 2011, **23**, 3944–3948.

43 Y. Chang, S.-T. Yang, J.-H. Liu, E. Dong, Y. Wang, A. Cao, Y. Liu and H. Wang, *Toxicol. Lett.*, 2011, **200**, 201–210.

44 J. Tian, J. Chen, C. Ge, X. Liu, J. He, P. Ni and Y. Pan, *Bioconjugate Chem.*, 2016, **27**, 1518–1524.

45 X. Liu, X. Zhang, M. Zhu, G. Lin, J. Liu, Z. Zhou, X. Tian and Y. Pan, *ACS Appl. Mater. Interfaces*, 2017, **9**, 279–285.

46 O. Akhavan, E. Ghaderi and A. Esfandiar, *J. Phys. Chem. B*, 2011, **115**, 6279–6288.

47 S. Kang, M. Herzberg, D. F. Rodrigues and M. Elimelech, *Langmuir*, 2008, **24**, 6409–6413.

48 S. Liu, L. Wei, L. Hao, N. Fang, M. W. Chang, R. Xu, Y. Yang and Y. Chen, *ACS Nano*, 2009, **3**, 3891–3902.

49 S. Liu, M. Hu, T. H. Zeng, R. Wu, R. Jiang, J. Wei, L. Wang, J. Kong and Y. Chen, *Langmuir*, 2012, **28**, 12364–12372.

50 E. L. K. Chng, Z. Sofer and M. Pumera, *Nanoscale*, 2014, **6**, 14412–14418.

51 K.-H. Liao, Y.-S. Lin, C. W. Macosko and C. L. Haynes, *ACS Appl. Mater. Interfaces*, 2011, **3**, 2607–2615.

52 E. L. K. Chng, C. K. Chua and M. Pumera, *Nanoscale*, 2014, **6**, 10792–10797.

53 D. K. Ji, Y. Zhang, Y. Zang, J. Li, G. R. Chen, X. P. He and H. Tian, *Adv. Mater.*, 2016, **28**, 9356–9363.

54 R. Foldbjerg, D. A. Dang and H. Autrup, *Arch. Toxicol.*, 2011, **85**, 743–750.

55 A. Casey, E. Herzog, F. Lyng, H. Byrne, G. Chambers and M. Davoren, *Toxicol. Lett.*, 2008, **179**, 78–84.

56 W. Hu, C. Peng, W. Luo, M. Lv, X. Li, D. Li, Q. Huang and C. Fan, *ACS Nano*, 2010, **4**, 4317–4323.

57 G. Duan, S.-G. Kang, X. Tian, J. A. Garate, L. Zhao, C. Ge and R. Zhou, *Nanoscale*, 2015, **7**, 15214–15224.

58 C. Ge, J. Tian, Y. Zhao, C. Chen, R. Zhou and Z. Chai, *Arch. Toxicol.*, 2015, **89**, 519–539.

59 W. Z. Teo, E. L. K. Chng, Z. Sofer and M. Pumera, *Chem.–Eur. J.*, 2014, **20**, 9627–9632.